Chemisorption of CO on N-doped Graphene on Ni(111)

*Giovanni Carraro §+, Edvige Celasco §+, Marco Smerieri +, Letizia Savio +, Gianangelo Bracco §,+, Mario Rocca §,+, Luca Vattuone §,+ **

+ CNR IMEM Unità Operativa di Genova, Via Dodecaneso 33, 16146 Genova (Italy)

§ Dipartimento di Fisica dell'Università degli Studi di Genova, Via Dodecaneso 33, 16146 Genova (Italy)

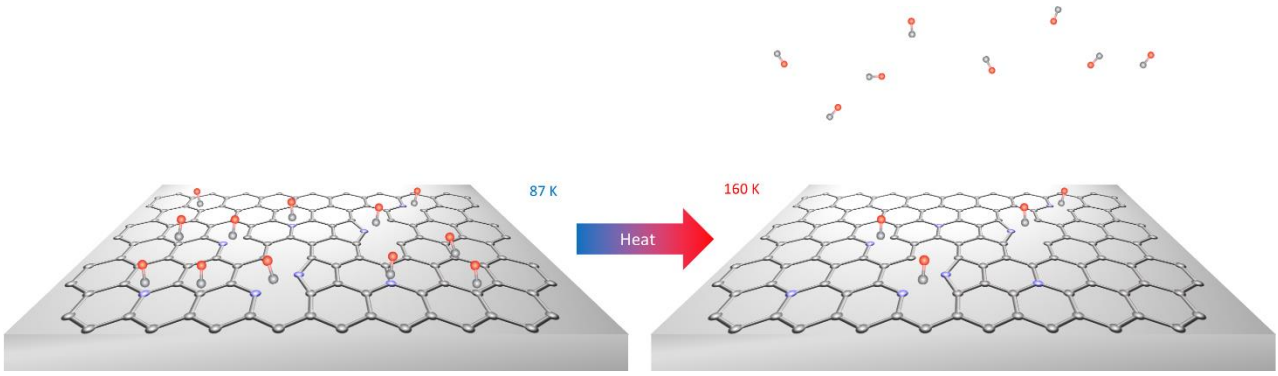

ABSTRACT:

The chemical reactivity of single layers of supported graphene (G) is affected by the nature of the underlying substrate: in particular CO chemisorption occurs on G/Ni(111), while graphene on Cu is inert. Here, we demonstrate experimentally that doping of the G layer with nitrogen atoms further increases the reactivity of the G/Ni(111) system towards CO. The doped layer is obtained by sputtering pristine G/Ni(111) with N_2^+ ions. For an ~11% dopant concentration, an additional electron energy loss at 238 meV appears in the HREEL spectra besides the loss around 256 meV present also on pristine G/Ni(111). The new feature corresponds to a CO species with a higher

desorption temperature and, consequently, a higher adsorption energy than the one forming on pristine G/Ni(111). At low coverage, the adsorption energy is estimated to be ~ 0.85 eV/molecule.

Keywords: Graphene, adsorption, carbon monoxide, vibrational spectroscopy, XPS

Introduction

Though pristine graphene is expected to be chemically inert, its interaction with gas phase molecular species has been reported in literature [1,2] not only for highly reactive species, such as aryl radicals [3,4], halogenated compounds [5] and atomic hydrogen [6], but also for small, less reactive molecules such as water [7].

Graphene (G) based sensors have been demonstrated to have sensitivities better than 1 part per million (ppm) for NO_2 and NH_3 [8,9], implying that these molecules adsorb, at least transiently, at the graphene surface. The physical effect at the basis of the sensing mechanism is the doping of the G layer induced by adsorption. The shift of the Dirac cone with respect to the Fermi energy and the related charge transfer modifies the density of carriers without significantly affecting their mobility, thus resulting in a modified conductivity. The magnitude of the effect and the n- or p-type of doping depends on the nature of the molecule. H_2O and NO_2 act, e.g., as acceptors of electrons while NH_3, CO and NO act as donors [8]. Due to the limited charge transfer between the molecule and the G-layer, the efficiency for CO detection is quite low. For G films and ribbons grown onto a Ni film supported on Si and then transferred onto a chip to test their sensitivity under practical conditions, the sensitive threshold came out to be 100 ppm of CO [10]. A twice as large value was achieved when operating the sensor at 573 K [10] but, since CO is toxic to human beings already in concentrations of 35 ppm, the current sensitivities are still insufficient for applications in safety issues [11]. More sensitive devices are thus required.

The achievable sensitivity depends ultimately on the adsorption energy of the target molecule at the surface of the active element. Such energy must be high enough to allow for an equilibrium coverage sufficient to produce a measurable signal but, possibly, low enough to allow operating the sensor at room temperature (RT). Theoretical calculations have estimated adsorption energies for simple molecules such as CO, NO, NO_2, NH_3 and H_2O on free standing graphene between 14 meV/molecule and 67 meV/molecule [12], i.e. values compatible with physisorption and in contrast with the observed high sensitivity reported for free-standing G-layer sensors at room temperature. Moreover, such sensors need to be annealed to 423 K to re-generate them after exposure to reactive gases [8], while the intrinsic response of graphene to ammonia drastically decreases after properly removing contaminants introduced during nanolithography [13]. This behaviour suggests the sensing effect to be related to some minority defect sites rather than to the pristine graphene layer [14] but, to the best of our knowledge, their identity is still unclear.

The adsorption properties of G-layers may be influenced by several factors such as, e.g., intrinsic doping induced by the presence of a strongly interactive substrate. Indeed, we have recently shown that weak CO chemisorption occurs at regular G sites (witnessed by STM inspection) for G/Ni(111), while under identical conditions G grown on polycrystalline Cu samples is totally inert [15,16]. The chemisorptive nature of the interaction is demonstrated by the redshift of the CO stretch frequency with respect to its gas phase value, by the presence of a CO-surface stretch at ~50 meV (close to the value observed for CO chemisorbed at other substrates) and by a desorption temperature T_{des}>150 K. From T_{des}, values of the heat of adsorption of ~0.58 eV/molecule and ~0.35 eV/molecule were estimated in the low coverage limit and for Θ_{CO}= 0.33 monolayers (ML, referred to the Ni lattice sites), respectively. Such values are compatible with an equilibrium

coverage of 0.1 ML at RT under a pressure of the order of 10 mbar of CO [16], thus suggesting a possible active role of G/Ni when it is used to support catalytically active nanoparticles.

As mentioned before, the role of defects is an important issue to be clarified in the investigation of the chemical activity of G-layers. Indeed, theoretical studies performed on free-standing graphene suggested a role of the low coordinated C atoms at isolated vacancy sites for CO and/or NO adsorption [17], while very little information is available for supported graphene layers [18–20]. Predictions of theory for the role of vacancies [17] were not confirmed by on purpose experiments [15] since we have recently shown that single vacancies are not responsible for the sensing activity of graphene supported on metals. In fact, C atoms at the vacancy edges are passivated by back-folding towards the metallic substrate and by the binding to the substrate atoms [21]. CO adsorption occurs thus only by CO intercalation when the binding to the underlying metal is strong enough [15]. Vacancies can otherwise be reactive in presence of a buffer layer, which decouples G from the substrate and reduces the possibility of back-bonding [22].

Another important parameter to be considered when studying adsorption properties is the doping of the G-layer. An enhanced chemical activity was predicted by first principle theoretical calculations, e.g., for B-doped graphene interacting with NO_2 and NH_3 [17]. Theorists proposed moreover that, while graphene vacancies cannot selectively sense CO in air, N-doped graphene could be an excellent candidate for this purpose [23] since pyridinic-like N-doped sites can adsorb this molecule but are inert towards N_2 and O_2. Adsorption should be accompanied by a large charge transfer, which would in turn provide a detectable signal for CO sensing. The calculated heat of adsorption for CO on N-doped graphene is 3.43 eV, to be compared to the value of 0.17 eV for the pristine layer. Even higher adsorption energies have been predicted for Al doped graphene [24].

The increased reactivity induced by doping of the G-film has been proved experimentally, e.g., for NH_3 in concentrations of 100 ppm at RT on P doped graphene [25]. More recently the key role of pyridinic N in the Oxygen Reduction Reaction has been demonstrated, too [26].

Depending on the doping site, different shifts of the graphene bands are expected: while pyridinic N would cause an upshift of the bottom of the π band, incorporation of N into the graphene lattice in substitutional sites (otherwise called graphitic N) would cause a shift in the opposite direction [27].

Here, we present an experimental study performed under controlled ultra-high vacuum (UHV) conditions aimed at clarifying the effect of doping with N atoms on the reactivity towards CO adsorption of a G/Ni(111) layer. In addition to the chemisorption channel open also for pristine G/Ni(111) [16], the presence of N atom dopants causes the appearance of a novel chemisorbed CO species. The latter is characterized by a CO stretch frequency in the range expected for bidentate CO and by an adsorption energy close to ~0.85 eV/molecule at low coverage, i.e. significantly higher than for CO at pristine G/Ni(111) sites.

Experimental section

Experiments were performed in a UHV chamber equipped with a high resolution electron energy loss spectrometer (HREELS – Delta0.5 by SPECS) and by a conventional, non monochromatized X-ray source (DAR400 Omicron) and hemispherical analyser (EA125 Omicron) for X-ray Photoelectron spectroscopy (XPS).

The Ni(111) crystal was cleaned by repeated sputtering (with 3 keV Ne^+ ions) and annealing (1283 K) cycles. Graphene was grown in situ by the thermal dehydrogenation of ethene catalysed by the Ni surface at T_g=823 K, (P=5 10^{-6} mbar 660 seconds), as described in more detail [15,16,28].

This procedure resulted in single-layer graphene domains up to a few tens of nm in size, as verified by LT-STM [16]. According to a recent XPS study, this protocol enables to obtain a high fraction of top-fcc graphene, which is the most reactive configuration for CO adsorption [28]. N-doping was introduced by bombarding the pristine G/Ni(111) single layer [29] with N_2^+ ions with 110 eV energy (the lowest energy attainable with our ion gun) at normal incidence and RT. The ion dose was varied to control the doping level and it is set to ~10^{15} ions/cm^2 in the present experiment. The layer was eventually annealed to 550 K to reduce the amount of implanted nitrogen. Higher temperature annealing was not performed to avoid the possible depletion of pyridinic N, as reported for G/Ir(111) [30]. CO was dosed by backfilling the chamber with a doser close to the sample [15,16,28].

The cleanliness of the Ni(111) substrate, the chemical nature of the graphene layer as well as the doping level were checked by XPS. Spectra were recorded using the Al K_α photon and the binding energy (E_B) was calibrated on the metallic Ni $2p_{3/2}$ photoemission peak, which is located at E_B=852.6 eV in absence of dissolved carbon [31]. In order to obtain quantitative information on the chemical composition, the spectra were fitted with an asymmetric Doniach-Sunjic line shape after subtracting a Shirley background. An asymmetry parameter α=0.08, intermediate between the one (0.1) typical of G/Ni(111) and the one found for G/Ni(111) after Au intercalation (0.061), was used [32]. Up to four components were necessary to reproduce the C1s line shape, while three components were employed to fit the N 1s region.

CO adsorption was monitored by HREELS. Spectra were recorded *in specular,* at 62° incidence with respect to the surface normal and at primary electron energy E=5 eV to enhance the sensitivity to adsorbed species. Thanks to the high dynamical dipole moment, CO can be detected already at

very low surface coverage. The spectra are normalized to the inelastic background around 300 meV.

RESULTS AND DISCUSSION

Figure 1 shows the X-ray photoemission spectra of the C1s and N 1s regions recorded after growth of the G/Ni(111) layer (bottom spectra) and after doping it by N_2^+ ion sputtering (top spectra). N_2^+ ion bombardment and annealing to 550 K causes a significant modification of the C 1s line with respect to the pristine graphene case: it broadens significantly and a shoulder develops at lower E_B. While the pristine G/Ni(111) can be described by a single C1s component centered at 284.7 eV, the N-doped layer clearly consists of different C species. Its line shape can be properly described only including additional components due to detached G (284.1 eV, ~28 %), to Ni_2C (283.4 eV, ~13 %) and to C bonded to N (285.5 eV, ~16 %). The ratio between the number of C atoms bonded to N and the number of C atoms *in graphene* is 18 %. The N1s spectrum demonstrates that N atoms are present in different configurations, in agreement with literature [29,33]. Indeed, as summarized in table I, components with E_B=397.1 eV, 398.3 eV, 400.5 eV are identified and assigned by comparison with literature to Ni nitride, to pyridinic N and to pyrrolic N. No intensity is found at $E_B \geq 400.6$ eV, i.e. in the energy range suitable for graphitic N. We deduce therefore that this nitrogen species is absent or present in negligible concentration in our sample. While the assignment of the two features at lower E_B is straightforward, the presence of pyrrolic N in higher concentration than graphitic N is at variance with the results of ref. [29], which reports a component at 400.7 eV ascribing it to graphitic N only.

The concentration of the different N species, estimated by fitting the N1s spectra with the components shown in Figure 1, is summarized in Table II. By comparing the areas of the N1s and

C1s peaks weighted by the corresponding photoemission cross sections [34] and neglecting photoelectron diffraction and emission angle effects, it is possible to estimate a N/C ratio of 19 %. Excluding nitride, which is not part of the N-doped G layer, the sum of pyridinic, pyrrolic and graphitic nitrogen amounts to ~11 %, a value in fair agreement with the estimated concentration (~18 %) of C atoms in graphene bound to nitrogen obtained from the fit of the C1s line. The latter is expected to be 2:1 given that both nitrogen in pyridinic and in pyrrolic sites are bonded with two carbon atoms each. Such finding supports the conclusion that the fraction of graphitic N is negligible: if a significant amount of graphitic N were present, the amount of C bonded to N should be even higher since in the substitutional configuration each N bonds to three C atoms.

Eventually, the so-obtained N-doped graphene layers were exposed to 40 L CO at RT and at 87 K. The corresponding HREEL spectra are shown in Figure 2, together with the spectrum recorded after exposing pristine G/Ni(111) to the same CO dose. No traces of adsorbed CO are observed after exposing the N-doped G/Ni(111) layer at RT, indicating that ion bombardment with 110 eV nitrogen ions does not open an adsorption channel at RT. This result is at variance with what we observed for CO adsorption at a Ne^+ ions sputtered G/Ni(111) [15]. In that case, CO intercalation and chemisorption on the Ni(111) substrate occurs, yielding an intense loss at 237 meV and a weaker one at 253 meV, both stable at least up to 350 K [15]. The occurrence of intercalation close to the N site can thus be excluded and the absence of CO adsorption at RT also rules out the presence of bare Ni patches in the present experiment [35–37].

Upon exposure of the N-doped G/Ni(111) system at 87 K to 1 L of CO, a doublet at 237 and 256 meV appears in the HREEL spectrum. Both losses can be ascribed to the internal stretch mode of CO molecules and thus indicate CO adsorption at two non-equivalent sites. Increasing the CO exposure to 40 L causes a negligible increase of the losses, indicating that a coverage close to

saturation is reached already at the lowest dose. CO adsorption is thus a non-activated process with a high sticking probability. The intensity of the CO stretch vibration at 256 meV is only 15 % lower than the corresponding one measured upon 40 L of CO exposure onto pristine G/Ni(111) (bottom spectrum in Figure 2), but it is red-shifted in energy by ~4 meV. It is therefore compatible with CO molecules in a mono-dentate configuration, i.e. in on-top position [38]. On the other hand, the weaker loss at ~238 meV, present only for the doped sample, is compatible with the internal stretch mode of doubly coordinated (i.e. bridge bonded) [38] CO. The additional broader losses around 48 meV and 97 meV are assigned to the CO-substrate stretch vibration and to water contamination, respectively.

In order to estimate the adsorption energy of the observed CO moieties, the thermal evolution of the HREEL spectra was recorded while the sample warms up (Figure 3A). The heating rate is not constant because, since the use of a heater is not compatible with the simultaneous recording of sequential HREEL spectra, the sample was annealed by switching off the cooling system. The 256 meV species starts to decrease immediately upon annealing, while the one at lower energy is stable up to 160 K and disappears below RT. Since both CO intercalated under G/Ni [15,36] and CO adsorbed on bare Ni(111) [35,36] desorb well above RT, we conclude that the observed losses correspond to CO admolecules at graphene sites.

The frequency of the mono-dentate species (254-256 meV) is close to the one observed on pristine G/Ni(111) (260 meV [16]), so we assign it to CO adsorbed at bare graphene sites. The slight redshift with respect to the pristine G case is due either to a larger charge transfer, and thus a possibly slightly stronger chemisorption, or to a lower local coverage or to a combination of both effects. By comparing the intensity (normalized to the background) of the 256 meV peak with the one found for pristine G/Ni(111), we can roughly estimate the coverage of mono-dentate CO to be

~85 % of the one reported for the CO-saturated pristine sample. Since in that case a local coverage of 0.33 ML (in ML of Ni(111)) was estimated from analysis of STM images, here we can assume a maximum coverage of~0.28 ML for the 256 meV species.

We assign the feature at 238 meV to CO adsorbed close to doped sites. From the intensity ratio between the two CO stretch peaks, which is initially between ¼ (Figure 2) and 1/3 (Figure 3), we deduce the coverage of the bidentate moiety to be ~0.10 ML, under the assumption that the dynamical dipole moments of the two species are comparable. The temperature dependence of the peak intensity (and hence of the coverage) of the two CO species is reported in Figure 3B together with simulations performed to estimate the CO desorption energy. Assuming an initial coverage of 0.10 ML and 0.28 ML for bi-dentate and mono-dentate species, respectively, and a pre-factor for desorption $\upsilon_{des} = 10^{13}$ Hz, the desorption energy could be estimated applying the following rate equation:

$$\frac{d\Theta}{dt} = -\upsilon_{des}\Theta\, e^{-\frac{E(\Theta)}{kT(t)}}$$

in which T(t) is the time dependence of the sample temperature obtained by allowing the sample to warm up by switching off the cooling system, k is the Boltzmann constant and E(Θ) is the coverage dependent desorption energy. We mention that fitting the data with a coverage independent heat of adsorption was not possible. Therefore, in absence of calorimetric data for this system, we assumed a linear dependence of E with coverage to account for the presence of repulsive interactions between the adsorbates [39]:

$$E(\Theta) = E(0) - a\Theta$$

Numeric integration of the related finite difference equation:

$$\Theta(t + \Delta t) = \Theta\,(t) - \upsilon_{des}\Theta(t)\, e^{-\frac{\bar{E(\Theta)}}{kT(t)}\Delta t}$$

gave the curves reported in Figure 3B (continuous lines) with the fitting parameters shown in table III. We observe that the temperature dependence of the 256 meV species is described reasonably well by the same values of the heat of adsorption obtained for pristine G/Ni(111). We thus conclude that the reason for the slightly lower frequency is most likely the lower local coverage.

On the contrary, the increase of the heat of adsorption for the bidentate CO molecules in proximity of a doped site is quite relevant. In the low coverage limit, it implies a lifetime of about 180 s at RT, to be compared with 0.2 ms for non-doped graphene. Even if such values can be affected by systematic errors due to the choice of the pre-factor for desorption, the substantial stabilization of adsorbed CO induced by N doping is evident.

The present study does not allow to determine which nitrogen species among those detected in the XPS spectrum of Figure1 are responsible for the stabilization of bidentate CO. However, nitride is ruled out since it is buried below graphene, so it is not part of the layer and it is expected to be a spectator. This conclusion is supported by the fact that the estimated coverage of bidentate CO (~0.10 ML) is close to the amount of N (11 %) included in the graphene layer (pyridinic and pyrrolic N). However, we cannot exclude that more than one CO molecule is stabilized by each dopant atom, implying then that only one N species may be active. Although additional experiments performed with different ratios of pyrrolic, pyridinic and, possibly, graphitic N species would be required to clarify this point, the identification of the active site with pyridinic and/or pyrrolic N is already evident. The possibility that the newly observed CO species is adsorbed at nickel carbide sites is ruled out because, in presence of Ni_2C, adsorbed CO should desorb between 290 and 320 K [36]. Finally, to the best of our knowledge, there are no surface science studies of adsorption of CO on nickel nitride but, for the chemically similar reduced Ni_2P,

CO desorbs above RT [40], at variance with observation in the present experiment. This suggests that also nickel nitride is not responsible for the observed CO species desorbing below RT.

Conclusions

We have shown by vibrational spectroscopy that, upon doping of a graphene monolayer supported on Ni(111) with N atoms, two chemisorbed CO species form. The dominant one, corresponding most likely to adsorption at non-doped sites, has a CO stretch frequency (256 meV) close to the one measured on a pristine G/Ni (111) sample (260 meV) and has the same desorption energy (0.54 eV/molecule in the zero coverage limit and 0.34 eV/molecule at 1/3 ML coverage[16]). The minority species, on the contrary, has a CO stretch frequency of 238 meV and a ~50% larger desorption energy. It is associated to CO admolecules sitting close to N-doped sites of pyridinic and/or pyrrolic nature. This work demonstrates that N doping enables stabilization of adsorbed CO at G/Ni(111), a result relevant for the graphene chemistry and for sensing applications.

AUTHOR INFORMATION

Corresponding Author

* Luca Vattuone, Dipartimento di Fisica dell'Università di Genova & IMEM-CNR Via Dodecaneso 33, 16416 Genova (Italy) Tel: +39-010-3536292- +39-010-3536544

Author Contributions

The experimental data were recorded by Giovanni Carraro, Marco Smerieri and Edvige Celasco. All authors contributed to the interpretation of the interpretation of the results and to the writing of the paper. All authors have given approval to the final version of the manuscript.

Funding Sources

We acknowledge funding by PRIN Project GRAF 20105ZZTSE_003, by the FIRB Futuro in Ricerca 2012 project N. RBFR128BEC_004, and by PRA 2013 and FRA 2017 from the University of Genova.

ABBREVIATIONS

G: graphene

n-doped G corresponds to N doped graphene

HREELS: High Resolution Electron Energy Loss Spectroscopy

XPS: X ray Photoelectron Spectroscopy

REFERENCES

[1] L. Kong, A. Enders, T.S. Rahman, P.A. Dowben, Molecular adsorption on graphene, J. Phys. Condens. Matter. 26 (2014) 443001. doi:10.1088/0953-8984/26/44/443001.

[2] Q. Fu, X. Bao, Surface chemistry and catalysis confined under two-dimensional materials, Chem. Soc. Rev. 46 (2017) 1842–1874. doi:10.1039/C6CS00424E.

[3] Q. Wu, Y. Wu, Y. Hao, J. Geng, M. Charlton, S. Chen, Y. Ren, H. Ji, H. Li, D.W. Boukhvalov, R.D. Piner, C.W. Bielawski, R.S. Ruoff, Selective surface functionalization at regions of high local curvature in graphene, Chem. Commun. 49 (2013) 677–679. doi:10.1039/c2cc36747e.

[4] Q.H. Wang, Z. Jin, K.K. Kim, A.J. Hilmer, G.L.C. Paulus, C.-J. Shih, M.-H. Ham, J.D. Sanchez-Yamagishi, K. Watanabe, T. Taniguchi, J. Kong, P. Jarillo-Herrero, M.S. Strano, Understanding and controlling the substrate effect on graphene electron-transfer chemistry via reactivity imprint lithography, Nat. Chem. 4 (2012) 724–732. doi:10.1038/nchem.1421.

[5] C. Morchutt, J. Björk, S. Krotzky, R. Gutzler, K. Kern, Covalent coupling via dehalogenation on Ni(111) supported boron nitride and graphene, Chem. Commun. 51 (2015) 2440–2443. doi:10.1039/C4CC07107G.

[6] W. Zhao, J. Gebhardt, F. Späth, K. Gotterbarm, C. Gleichweit, H. Steinrück, A. Görling, C. Papp, Reversible Hydrogenation of Graphene on Ni(111)-Synthesis of “Graphone,” Chem. - A Eur. J. 21 (2015) 3347–3358. doi:10.1002/chem.201404938.

[7] A. Politano, M. Cattelan, D.W. Boukhvalov, D. Campi, A. Cupolillo, S. Agnoli, N.G.

Apostol, P. Lacovig, S. Lizzit, D. Farias, G. Chiarello, G. Granozzi, R. Larciprete, D. Farías, G. Chiarello, G. Granozzi, R. Larciprete, Unveiling the Mechanisms Leading to H2 Production Promoted by Water Decomposition on Epitaxial Graphene at Room Temperature, ACS Nano. 10 (2016) 4543–4549. doi:10.1021/acsnano.6b00554.

[8] A.K. Geim, K.S. Novoselov, The rise of graphene, Nat. Mater. 6 (2007) 183–191. doi:10.1038/nmat1849.

[9] T.O. Wehling, K.S. Novoselov, S. V Morozov, E.E. Vdovin, M.I. Katsnelson, a K. Geim, a I. Lichtenstein, Molecular doping of graphene., Nano Lett. 8 (2008) 173–7. doi:10.1021/nl072364w.

[10] E. Kayhan, R.M. Prasad, A. Gurlo, O. Yilmazoglu, J. Engstler, E. Ionescu, S. Yoon, A. Weidenkaff, J.J. Schneider, Synthesis, Characterization, Electronic and Gas-Sensing Properties towards H2 and CO of Transparent, Large-Area, Low-Layer Graphene, Chem. - A Eur. J. 18 (2012) 14996–15003. doi:10.1002/chem.201201880.

[11] T. Wang, D. Huang, Z. Yang, S. Xu, G. He, X. Li, N. Hu, G. Yin, D. He, L. Zhang, A Review on Graphene-Based Gas/Vapor Sensors with Unique Properties and Potential Applications, Nano-Micro Lett. 8 (2016) 95–119. doi:10.1007/s40820-015-0073-1.

[12] O. Leenaerts, B. Partoens, F. Peeters, Adsorption of H2O, NH3, CO, NO2, and NO on graphene: A first-principles study, Phys. Rev. B. 77 (2008) 125416. doi:10.1103/PhysRevB.77.125416.

[13] Y. Dan, Y. Lu, N.J. Kybert, Z. Luo, A.T.C. Johnson, Intrinsic Response of Graphene Vapor Sensors, Nano Lett. 9 (2009) 1472–1475. doi:10.1021/nl8033637.

[14] A. Eftekhari, H. Garcia, The necessity of structural irregularities for the chemical applications of graphene, Mater. Today Chem. 4 (2017) 1–16. doi:10.1016/j.mtchem.2017.02.003.

[15] E. Celasco, G. Carraro, A. Lusuan, M. Smerieri, J. Pal, M. Rocca, L. Savio, L. Vattuone, CO chemisorption at vacancies of supported graphene films: a candidate for a sensor?, Phys. Chem. Chem. Phys. 18 (2016) 18692–18696. doi:10.1039/C6CP02999J.

[16] M. Smerieri, E. Celasco, G. Carraro, A. Lusuan, J. Pal, G. Bracco, M. Rocca, L. Savio, L. Vattuone, Enhanced Chemical Reactivity of Pristine Graphene Interacting Strongly with a Substrate: Chemisorbed Carbon Monoxide on Graphene/Nickel(1 1 1), ChemCatChem. 7 (2015) 2328–2331. doi:10.1002/cctc.201500279.

[17] Y.-H. Zhang, Y. Chen, K.-G. Zhou, C. Liu, J. Zeng, H. Zhang, Y. Peng, Improving gas sensing properties of graphene by introducing dopants and defects: a first-principles study, Nanotechnology. 20 (2009) 185504. doi:10.1088/0957-4484/20/18/185504.

[18] A. Ambrosetti, P.L. Silvestrelli, Communication: Enhanced chemical reactivity of graphene on a Ni(111) substrate, J. Chem. Phys. 144 (2016) 111101. doi:10.1063/1.4944090.

[19] L. Ferrighi, C. Di Valentin, Oxygen reactivity on pure and B-doped graphene over crystalline Cu(111). Effects of the dopant and of the metal support, Surf. Sci. 634 (2015) 68–75. doi:10.1016/j.susc.2014.11.001.

[20] A. Ambrosetti, P.L. Silvestrelli, Toward Tunable CO Adsorption on Defected Graphene: The Chemical Role of Ni(111) and Cu(111) Substrates, J. Phys. Chem. C. (2017) acs.jpcc.7b06243. doi:10.1021/acs.jpcc.7b06243.

[21] M.M. Ugeda, D. Fernández-Torre, I. Brihuega, P. Pou, A.J. Martínez-Galera, R. Pérez, J.M. Gómez-Rodríguez, Point defects on graphene on metals, Phys. Rev. Lett. 107 (2011) 116803. doi:10.1103/PhysRevLett.107.116803.

[22] R.A. Bueno, J.I. Martínez, R.F. Luccas, N.R. del Árbol, C. Munuera, I. Palacio, F.J.

Palomares, K. Lauwaet, S. Thakur, J.M. Baranowski, W. Strupinski, M.F. López, F. Mompean, M. García-Hernández, J.A. Martín-Gago, Highly selective covalent organic functionalization of epitaxial graphene, Nat. Commun. 8 (2017) 15306. doi:10.1038/ncomms15306.

[23] C. Ma, X. Shao, D. Cao, Nitrogen-doped graphene as an excellent candidate for selective gas sensing, Sci. China Chem. 57 (2014) 911–917. doi:10.1007/s11426-014-5066-2.

[24] Z. Ao, J. Yang, S. Li, Q. Jiang, Enhancement of CO detection in Al doped graphene, Chem. Phys. Lett. 461 (2008) 276–279. doi:10.1016/j.cplett.2008.07.039.

[25] F. Niu, L.-M. Tao, Y.-C. Deng, Q.-H. Wang, W.-G. Song, H. Feng, X.J. Huang, S. Alvarez-Garcia, A. de Andres, F. Pariente, E. Lorenzo, X.H. Bao, Phosphorus doped graphene nanosheets for room temperature NH3 sensing, New J. Chem. 38 (2014) 2269. doi:10.1039/c4nj00162a.

[26] D. Guo, R. Shibuya, C. Akiba, S. Saji, T. Kondo, J. Nakamura, Active sites of nitrogen-doped carbon materials for oxygen reduction reaction clarified using model catalysts, Science (80-.). 351 (2016) 361–365. doi:10.1126/science.aad0832.

[27] R.J. Koch, M. Weser, W. Zhao, F. Viñes, K. Gotterbarm, S.M. Kozlov, O. Höfert, M. Ostler, C. Papp, J. Gebhardt, H.-P.P. Steinrück, A. Görling, T. Seyller, Growth and electronic structure of nitrogen-doped graphene on Ni(111), Phys. Rev. B. 86 (2012) 75401. doi:10.1103/PhysRevB.86.075401.

[28] E. Celasco, G. Carraro, M. Smerieri, L. Savio, M. Rocca, L. Vattuone, Influence of growing conditions on the reactivity of Ni supported graphene towards CO, J. Chem. Phys. 146 (2017) 104704. doi:10.1063/1.4978234.

[29] W. Zhao, O. Höfert, K. Gotterbarm, J.F. Zhu, C. Papp, H.-P. Steinrück, Production of Nitrogen-Doped Graphene by Low-Energy Nitrogen Implantation, J. Phys. Chem. C. 116 (2012) 5062–5066. doi:10.1021/jp209927m.

[30] A. Sala, G. Zamborlini, T.O. Menteş, A. Locatelli, T.O. Mente??, A. Locatelli, Fabrication of 2D Heterojunction in Graphene via Low Energy N_2^+ Irradiation, Small. 11 (2015) 5927–5931. doi:10.1002/smll.201501473.

[31] R.S. Weatherup, B.C. Bayer, R. Blume, C. Baehtz, P.R. Kidambi, M. Fouquet, C.T. Wirth, R. Schlögl, S. Hofmann, On the Mechanisms of Ni-Catalysed Graphene Chemical Vapour Deposition, ChemPhysChem. 13 (2012) 2544–2549. doi:10.1002/cphc.201101020.

[32] T. Susi, T. Pichler, P. Ayala, X-ray photoelectron spectroscopy of graphitic carbon nanomaterials doped with heteroatoms, Beilstein J. Nanotechnol. 6 (2015) 177–192. doi:10.3762/bjnano.6.17.

[33] D. Usachov, O. Vilkov, A. Grüneis, D. Haberer, A. Fedorov, V.K. Adamchuk, a B. Preobrajenski, P. Dudin, A. Barinov, M. Oehzelt, C. Laubschat, D. V Vyalikh, Nitrogen-doped graphene: efficient growth, structure, and electronic properties., Nano Lett. 11 (2011) 5401–7. doi:10.1021/nl2031037.

[34] J.J. Yeh, I. Lindau, Atomic subshell photoionization cross sections and asymmetry parameters: $1 \leqslant Z \leqslant 103$, At. Data Nucl. Data Tables. 32 (1985) 1–155. doi:10.1016/0092-640X(85)90016-6.

[35] S.L. Tang, M.B. Lee, Q.Y. Yang, J.D. Beckerle, S.T. Ceyer, Bridge/atop site conversion of CO on Ni(111): Determination of the binding energy difference, J. Chem. Phys. 84 (1986) 1876. doi:10.1063/1.450435.

[36] M. Wei, Q. Fu, Y. Yang, W. Wei, E. Crumlin, H. Bluhm, X. Bao, Modulation of Surface Chemistry of CO on Ni(111) by Surface Graphene and Carbidic Carbon, J. Phys. Chem. C.

119 (2015) 13590–13597. doi:10.1021/acs.jpcc.5b01395.
[37] J.C. Bertolini, B. Tardy, Vibrational EELS studies of CO chemisorption on clean and carbided (111), (100) and (110) nickel surfaces, Surf. Sci. 102 (1981) 131–150. doi:10.1016/0039-6028(81)90312-5.
[38] M. Gajdo, A. Eichler, J. Hafner, CO adsorption on close-packed transition and noble metal surfaces: trends from *ab initio* calculations, J. Phys. Condens. Matter. 16 (2004) 1141–1164. doi:10.1088/0953-8984/16/8/001.
[39] Y.Y. Yeo, L. Vattuone, D.A. King, Calorimetric investigation of NO and CO adsorption on Pd{100} and the influence of preadsorbed carbon, J. Chem. Phys. 106 (1997) 1990–1996. doi:10.1063/1.473306.
[40] K.A. Layman, M.E. Bussell, Infrared spectroscopic investigation of thiophene adsorption on silica-supported nickel phosphide catalysts, J. Phys. Chem. B. 108 (2004) 15791–15802. doi:10.1021/jp047882z.
[41] H.M. Jeong, J.W. Lee, W.H. Shin, Y.J. Choi, H.J. Shin, J.K. Kang, J.W. Choi, Nitrogen-doped graphene for high-performance ultracapacitors and the importance of nitrogen-doped sites at basal planes., Nano Lett. 11 (2011) 2472–7. doi:10.1021/nl2009058.
[42] L. Qu, Y. Liu, J.-B. Baek, L. Dai, Nitrogen-doped graphene as efficient metal-free electrocatalyst for oxygen reduction in fuel cells., ACS Nano. 4 (2010) 1321–6. doi:10.1021/nn901850u.

FIGURE CAPTIONS

Figure 1 C 1s (left) and N 1s (right) photoemission spectra recorded: (bottom spectra) after growth of the graphene film; (top spectra) after N-doping by N_2^+ ion bombardment (ion dose of ~10^{15} ions/cm^2) and subsequent annealing to 550 K

Figure 2. HREEL spectra showing CO adsorption at pristine G/Ni(111) (from ref. [16], bottom spectrum) and at N-doped G/Ni(111) for different T and CO dose, as discussed in the text. The data are normalized to the inelastic background around 300 meV.

Figure 3. A: HREEL spectra recorded sequentially on the N-doped G/Ni(111) layer exposed to 40 L of CO at T= 87 K while slowly warming up after switching off the cooling system. The temperature readings correspond to the average of T at the beginning and at the end of each spectrum. The N_2^+ dose is ~10^{15} ions/cm^2, yielding an N doping of ~11 % as estimated by XPS. B: Coverage of the two CO moieties (derived from the area of the CO-stretch peaks in HREELS) vs. crystal temperature.

	NG/Ni(111) [33]	NG/Ni(111) [29]	NG/Ni(111) [27]	HOPG [26]	NG (from GO) [41]	NG/Ni film [42]	Present study
Pyridinic	398.2-399.3	398.7	399	398.5	398.5	398.3	398.3
Pyrrolic	400.1-400.5			400.1	400.1	400.5	400.5
Graphitic		400.7	400.6	401.0	401.5		___
Nickel nitride		397.3					397.1

Table I *N1s binding energy (in eV) of the different N species according to recent literature: for N doped (NG) G grown on Ni(111), for different kinds of HOPG, for NG obtained from graphene oxide (GO) and for NG on a Ni film and for the present results.*

Protocol	Doping	N_{nitr}/N_{tot}	N_{pyr}/N_{tot}	N_{pyrr}/N_{tot}	N_g/N_{tot}
N_2^+ ion bombardment & flash to 550 K	11 %	43 %	41 %	16 %	~ 0 %

Table II *Doping level (defined as:* $(N_{pyr}+N_g+N_{pyrr})/(C_g+N_{pyr}+N_g+N_{pyrr})$*) and fraction of the different kinds (substitutional:* N_g*, pyridinic:* N_{pyr}*; pyrrolic:* N_{pyrr} *and nitride:* N_{nitr}*) of N atoms as determined by XPS. It is apparent that 43 % of the total amount of N is in nitride form and is thus*

not part of the G layer. We can estimate an uncertainty of ~ 2% on the concentration values reported in the table.

	E(Θ=0) (eV/molecule)	E($\Theta = \Theta_i$) (eV/molecule)	Θ_i (ML)
Monodentate CO (256 meV)	0.54	0.34	0.28
Bidentate CO (238 meV)	0.85	0.50	0.10

Table III. *Desorption energy for the single and double coordinated CO moiety, as obtained by fitting the temperature dependence of the corresponding CO stretch intensity (see text).*

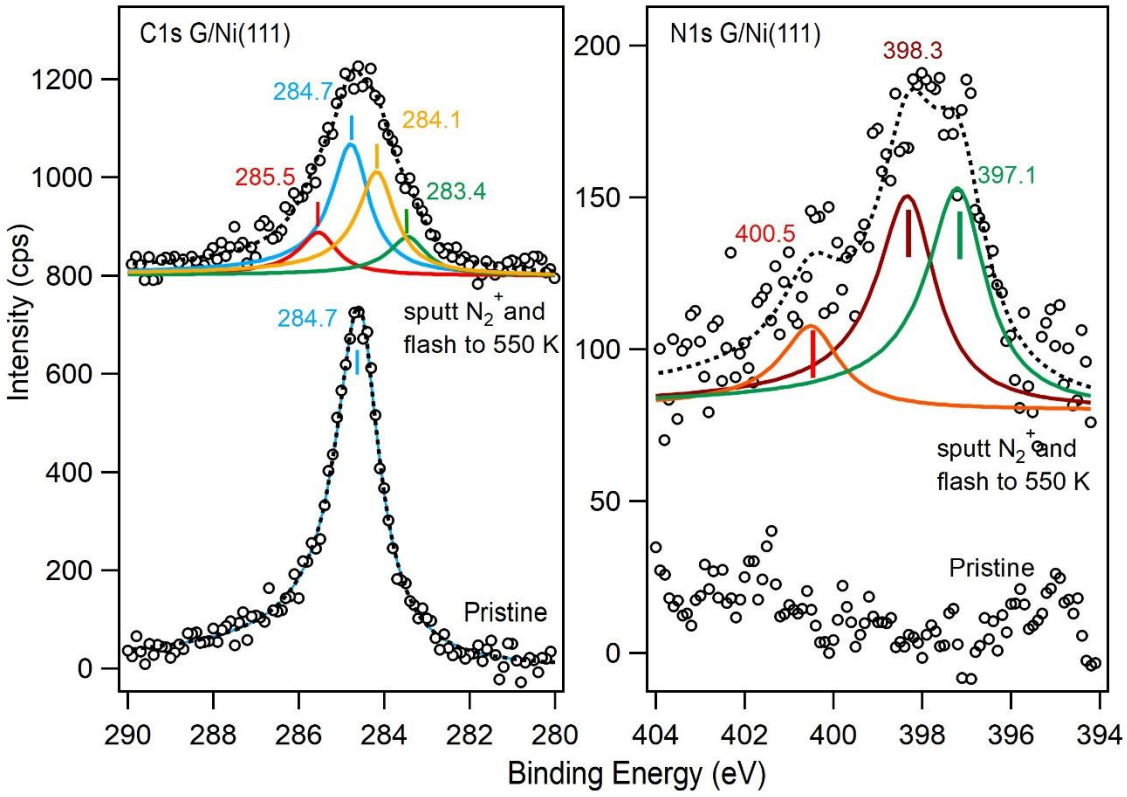
C1s G/Ni(111)
284.7
284.1
285.5
283.4
sputt N2+ and
flash to 550 K
284.7
Pristine
Intensity (cps)
1200
1000
800
600
400
200
0
290
288
286
284
282
280
N1s G/Ni(111)
398.3
397.1
400.5
sputt N2+ and
flash to 550 K
Pristine
200
150
100
50
0
404
402
400
398
396
394
Binding Energy (eV)

Figure 1

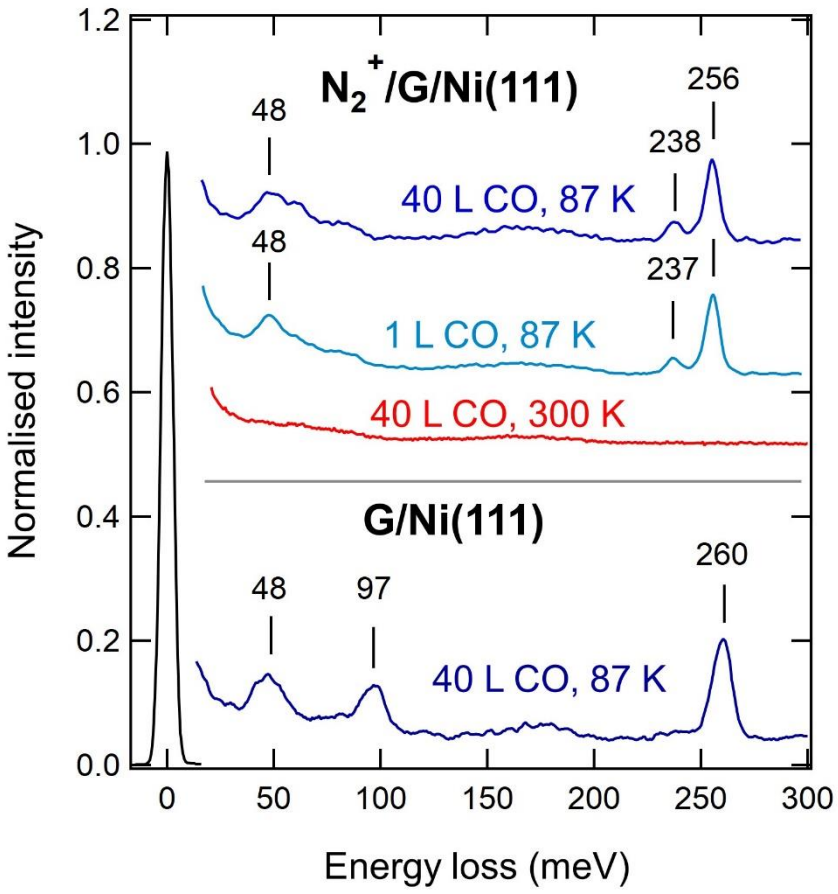
N_2^+/G/Ni(111)
48
256
238
40 L CO, 87 K
48
237
1 L CO, 87 K
40 L CO, 300 K
G/Ni(111)
260
48
97
40 L CO, 87 K
Normalised intensity
Energy loss (meV)
0.0
0.2
0.4
0.6
0.8
1.0
1.2
0
50
100
150
200
250
300

Figure 2

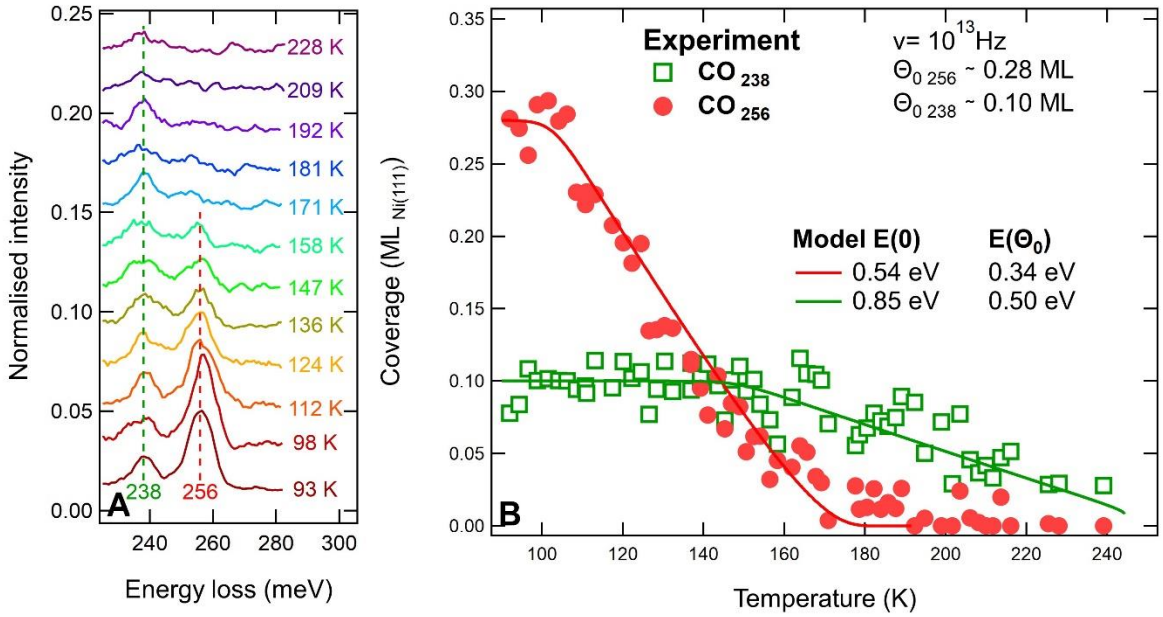
Normalised intensity
0.25
0.20
0.15
0.10
0.05
0.00
228 K
209 K
192 K
181 K
171 K
158 K
147 K
136 K
124 K
112 K
98 K
93 K
238
256
A
240
260
280
300
Energy loss (meV)
Coverage (ML Ni(111))
0.35
0.30
0.25
0.20
0.15
0.10
0.05
0.00
Experiment
CO 238
CO 256
v= 10^13 Hz
Θ0 256 ~ 0.28 ML
Θ0 238 ~ 0.10 ML
Model E(0)
E(Θ0)
0.54 eV
0.34 eV
0.85 eV
0.50 eV
B
100
120
140
160
180
200
220
240
Temperature (K)

Figure 3